

Chapter 5

Photocatalytic Hydrogen Production with Visible Light Using Nanocomposites of CdS and Niobium Oxide

Abstract

Niobium oxides (KNbO_3 , $\text{K}_4\text{Nb}_6\text{O}_{17}$) were combined with nanosize CdS particles and Ni to produce catalysts that could produce H_2 gas from water/ethanol solutions using visible light. Ni doping was shown to affect Nb–O bonding states, and to compete with Cd for ion exchange sites, although the Ni/CdS doped catalysts still showed a higher photocatalytic activity than with CdS doping alone. XPS studies showed the loss of excess Cd^{2+} , but not sulfur, during the course of the photoreaction for the KNbO_3 catalysts, but significant loss of both Cd and S for the $\text{K}_4\text{Nb}_6\text{O}_{17}$ catalysts.

Introduction

Perovskite structure transition metal oxides such as niobium-based semiconductors are molecules of interest in photocatalytic water splitting studies due to their layered crystal structure and ion exchange properties. One such material is KNbO_3 , an orthorhombic crystal that possesses the largest nonlinear coefficients for wavelength conversion of all commercially available inorganic materials. The photocatalytic properties of KNbO_3 have been studied using UV light,^{1,2} but there have been no reports of modified KNbO_3 catalysts for use in visible light photocatalysis. A more in-depth studied material has been another niobate semiconductor, $\text{K}_4\text{Nb}_6\text{O}_{17}$. The structure of $\text{K}_4\text{Nb}_6\text{O}_{17}$ consists of sheets made of two planes of NbO_6 octahedra linked with one-half of the K atoms.³ The potassium ion is easily exchanged by other metal ions to produce nanocomposites consisting of a Nb_6O_{17} host layer and nanoscale particles incorporated in the interlayer.⁴ The photocatalytic activity of $\text{K}_4\text{Nb}_6\text{O}_{17}$ toward water splitting was first reported 20 years ago by Domen and colleagues.⁵ They saw hydrogen production from $\text{K}_4\text{Nb}_6\text{O}_{17}$ in degassed water/alcohol solutions under UV irradiation, and increased activity with dopants such as H^+ and NiO .⁶ Since that time, a few groups have looked at combining CdS and/or Ni with $\text{K}_4\text{Nb}_6\text{O}_{17}$ particles to produce visible light hydrogen evolution.^{7,8}

In our laboratory, the creation of visible light catalysts comprised of Ni/CdS/ KNbO_3 is an area of ongoing research.⁹ In this study, the same techniques we developed for the KNbO_3 catalysts were applied to create Ni/CdS/ $\text{K}_4\text{Nb}_6\text{O}_{17}$ catalysts. Catalyst structure was confirmed by XRD and SEM, and hydrogen evolution was measured using several types of $\text{K}_4\text{Nb}_6\text{O}_{17}$ catalysts. In addition, the elemental

composition and bonding environment of both the KNbO_3 and $\text{K}_4\text{Nb}_6\text{O}_{17}$ catalysts were examined by XPS and FTIR.

Experimental

Instrumentation

UV-vis diffuse reflectance spectra were recorded on a Shimadzu UV-2101PC with an integrating sphere attachment (Shimadzu ISR-260), using Ba₂SO₄ powder as an internal reference. BET surface area measurements were performed on a Micromeritics Gemini 2360 Analyzer. Diffuse reflectance infrared fourier transform (DRIFT) spectra were acquired using a Bio-Rad FTS-45 spectrometer with a liquid N₂-cooled MCT detector. Spectra were collected at 8 cm⁻¹ resolution using a Spectra-Tech Collector diffuse-reflectance accessory. The solid samples were held in the sample cup of a Spectra-Tech high temperature environmental chamber (HTEC) that could be resistively heated to 1000 K (±1 K), and the chamber evacuated to 10 μTorr.

SEM images were taken on a LEO 1550VP FESEM. XRD spectra were recorded on a Phillips X'Pert PRO X-ray diffraction system. XPS experiments were performed in an M-probe surface spectrometer (VG Instruments) using monochromatic Al K_α X-rays (1486.6 eV). Liquid reaction products were analyzed by a Hewlett-Packard 6890 GC - 5973 MSD System with an Agilent 6890 series automatic liquid sampler. For headspace gas measurements, the photoreactor was connected to a pump-driven recirculating gas flow system, and measurements were taken with a Balzers Prisma QMS 200 quadropole mass spectrometer.

Photolysis experiments were performed by using the collimated output of a high-pressure Hg-Xe arc lamp as a light source. The light beam was passed through an IR filter, a focusing lens and a 400 nm cutoff filter before reaching the reactor. The reactor was cooled by a fan to keep it at room temperature. Since it is well known that colloidal

CdS suspensions undergo photocorrosion¹⁰⁻¹² and photocatalytic dissolution¹³⁻¹⁷ under oxic conditions, the H₂ production experiments were carried out under an argon atmosphere. All photolysis reactors were purged with Ar gas for 30 minutes in order to eliminate O₂.

H₂ was measured using gas chromatography (HP 5890 Series II) with a thermal conductivity detector (TCD). Due to similar conductivity values for He and H₂, nitrogen was used as a carrier gas. The separations were achieved with a molecular sieve column (30 m × 0.32 mm × 12.00 μm). The gas chromatograph oven temperature was 30 °C, as this was found to be the best temperature for spatial resolution between Ar (reactor purge gas) and H₂. Calibration curves were linear over a broad range of H₂ concentrations.

For photolysis experiments, unless otherwise specified, the catalyst loading was 0.2g, the reaction solution was 50 mL of 50:50 ethanol/water, and the lamp power was 500 W. Aliquots of the reactor's headspace gas (total headspace volume = 100 mL) were syringed out in 50μL volumes through a rubber septum. Samples were taken every 8-12 hours, and several samples were taken at each time point to ensure accuracy.

Synthesis of K₄Nb₆O₁₇

The two main methods of synthesizing K₄Nb₆O₁₇ are either by hydrothermal methods^{2,18,19} or by a high-temperature solid-state reaction.^{4,20-23} One attempt at a hydrothermal synthesis was made. Following the method of Liu et al.,¹⁸ 2g of Nb₂O₅ was combined with 40 mL of 0.5 M KOH solution, placed into a sealed Teflon pressure vessel, and heated at 180 °C for 4 days. However, XRD indicated that the starting niobate material had not reacted, perhaps because the synthesis temperature was too low; other researchers have indicated that a temperature of greater than 200 °C is needed.² The

remaining synthesis attempts were made using the solid-state reaction method, using K_2CO_3 and Nb_2O_5 as the starting materials. As the literature varied upon the synthesis conditions, a range of temperatures (1150 to 1300 °C) and starting material ratios (1:1.3 to 1:1.5) were used. The starting materials were ground with a mortar and pestle for 30 minutes, and at times acetone was added to aid the mixing process. The mixed powder was then compressed into a wafer form by a bench press operating at 3000 psi. The wafer was then broken into a few pieces, placed in a ceramic crucible, and inserted into a high temperature oven. It was found that any synthesis attempts above 1200 °C caused the solid mixture to melt. The successfully synthesized materials were examined by XRD, as shown in figure 5.1; many of the $K_4Nb_6O_{17}$ XRD spectra in the literature have poor resolution, however our sample closely matches one of the reports with higher resolution data.¹⁸ The best synthesized material was made using a stoichiometric molecular ratio (1:1.5) of starting materials, a temperature ramp rate of 200 °C/hour, a dwell temperature of 1150 °C, and a dwell time of 10 hours.

Synthesis of $H^+/K_4Nb_6O_{17}$

Following a procedure reported by Abe et al.,²⁴ $K_4Nb_6O_{17}$ was placed in a solution of 0.5 N H_2SO_4 and stirred for several days. The color of the solid $K_4Nb_6O_{17}$ turned from white to slightly brown over the course of the acid treatment. The solid product was filtered by water funnel, but during filtration, it was observed that a small portion of white product stuck to the walls of the filter funnel, and was only able to be washed down into the filter by addition of ethanol, indicating that this solid was non-polar. Less than 5% of sample mass was in the white, non-polar form.

Synthesis of $CdS/Ni/K_4Nb_6O_{17}$ Composites

Nickel coated $K_4Nb_6O_{17}$ powders were obtained by first treating the pure $K_4Nb_6O_{17}$ sample with $Ni(NO_3)_2$ in water, in order to ion-exchange Ni^{2+} with K^+ atoms in the catalyst. The total Ni mass was equal to 0.1% of the catalyst mass; this mass ratio was selected on the basis of previous success with the $KNbO_3$ catalysts. After 1 day of stirring, the water suspensions were filtered, washed and dried. The $Ni^{2+}/K_4Nb_6O_{17}$ sample was then reduced in a H_2 atmosphere at $500\text{ }^\circ\text{C}$ for 2 hours, followed by partial reoxidation in an O_2 atmosphere at $200\text{ }^\circ\text{C}$ for 1 hour, to form $Ni/K_4Nb_6O_{17}$. The actual form of the Ni, whether in elemental form or NiO, was not able to be determined, as Ni content was too low to be observed by XPS. It is likely that both forms exist, given that the sample is subject to both reducing and oxidizing conditions.

Cadmium sulfide was then synthesized within the layers of $K_4Nb_6O_{17}$ by the direct reaction of ion-exchanged Cd^{2+} with aqueous S^{2-} . One gram of $K_4Nb_6O_{17}$ was added to a 50 mL solution of ethanol containing 1×10^{-2} M cadmium acetate. The covered solution was stirred for 48 hours. A 50 mL solution of ethanol containing 1×10^{-2} M sodium sulfide was prepared in a Vacuum Atmospheres glove box. The sodium sulfide solution was slowly added to the cadmium acetate solution while stirring, resulting in a yellow-colored solution. The resulting solution was covered and stirred for 24 hours. The pH of this solution was between pH 6.0 to 6.5. The catalyst was then removed from solution by vacuum filtration, washed several times with ethanol, and dried overnight in an oven at $100\text{ }^\circ\text{C}$. The yield from this procedure was always greater than 90%.

The same procedure was applied to the $H^+/K_4Nb_6O_{17}$, however after H_2/O_2 gas treatment, the sample color seemed charred, and the color was non-uniform. And after the addition of CdS nanoparticles, the catalyst color was also non-uniform, indicating

poor adhesion of CdS.

Results and Discussion

KNbO₃

KNbO₃ catalysts that were previously shown to have high photocatalytic activity⁹ were examined spectroscopically to learn more about the changes that occur to the catalyst during the synthesis process as well as during the photoreaction. The initial KNbO₃ material was synthesized using two different molar ratios of the starting materials (either 1:1 or 1.1:1 ratio of Nb₂O₅ to K₂CO₃). Figure 5.2 shows DRIFT spectrum for a CdS/Ni/KNbO₃ catalyst which had been prepared from 1.1:1 KNbO₃, as well as the spectrum of solid CdS. The CdS peak at 1150 cm⁻¹ for the CdS/Ni/KNbO₃ catalyst is much sharper than the solid CdS peak in the same region, indicating nanosize CdS particles, as decreased particle size leads to sharper IR peak width. For catalysts prepared with 1:1 KNbO₃, no such sharp CdS peak was seen by FTIR. SEM images had indicated that the 1.1:1 KNbO₃ had at least a partially layered structure, somewhere in between pure crystalline KNbO₃ and the layered structure of K₄Nb₆O₁₇. Thus the nanosize CdS is likely only formed between the layers, as it is only seen in the layered materials.

Figure 5.3 shows the DRIFT spectra for two different Ni-doped catalysts (CdS/Ni/KNbO₃ and Ni_{1.1}K_{0.9}NbO₃), as well as for KNbO₃, in the strongly absorbing metal-oxygen bonding region. Comparing KNbO₃ to the Ni-doped catalyst prepared by ion-exchange (CdS/Ni/KNbO₃), the proportion of the higher-energy Nb–O edge species at 900 cm⁻¹ increases relative to the lower-energy bridged O–Nb–O species at 831 cm⁻¹. Since the frequency of the absorptions does not change, it is likely that the reduction in O–Nb–O is due to a physical effect, rather than a change in chemical bonding, as this

would effect the dipole moment. It is possible that the some of the 3 atom O–Nb–O stretching vibrations are inhibited by neighboring Ni atoms.

Comparing KNbO_3 to the Ni-doped catalyst prepared by direct incorporation of Ni during KNbO_3 synthesis ($\text{Ni}_{.1}\text{K}_{.9}\text{NbO}_3$), the absorption peaks for both Nb–O species are shifted to higher energy by 40 cm^{-1} . This result indicates that Ni doping increases catalyst defect intensity. Ni, with an ionic radius of 0.69 angstroms, is half the size of K ions, which have an ionic radius of 1.38 angstroms. Therefore it is not surprising that substitution of Ni for K leads to strain on the catalyst structure and an increase in higher-energy Nb–O sites.

In an attempt to gain insight into liquid products that may form during the reaction, a photolysis experiment using CdS/Ni/KNbO_3 was performed, and the reaction mixture was analyzed by GC/MS. Due to the necessity to break purge to collect liquid samples, it was difficult to monitor the reaction mixture real time or to collect sample points during the course of the reaction. Instead, one sample point was taken 30 minutes into the reaction, at which point the reactor was purged again with Ar, and the photocatalysis restarted. The reaction was run for an additional 11.5 hours, giving 12 total hours of reaction time. At the end of the reaction, the reaction mixture was immediately analyzed, and it was again analyzed after 30 minutes. Due to the high concentration of ethanol, it was impossible to quantitatively measure ethanol loss. Three other species were observed in measurable quantity, and they were identified by their MS fragments as methanol, ethyl acetate and methyl isobutyl ketone. These three species were the denaturants added to the commercial ethanol in minute amounts. Thus, it appears no new organic species were generated during the course of the reaction. As the

methyl isobutyl ketone peak overlapped with the ethanol peak, it was possible to examine only methanol and ethyl acetate. Figure 5.4 shows the data points collected at the beginning and end segments of the experiment. An immediate loss (~25%) of ethyl acetate is seen within 30 minutes, and over the course of the reaction, there is a net loss of close to 40% of the initial ethyl acetate concentration. Conversely, methanol concentration is seen to slightly increase (~10%) during the course of the reaction. Concentrations of both species did not change greatly during the period of reexposure to air after the end of the photolysis. It is interesting to note that there is not complete loss of ethyl acetate, and that methanol concentration did not increase much. The data provide indirect evidence for the theory that most ethanol survives the reaction, as there was no sign of ethanol breakdown products other than methanol, and the methanol concentration only increased slightly. And the fact that ethyl acetate, a species more likely to be photochemically degraded than ethanol due to the potential for decarboxylation, is not completely lost also supports this theory. An expected product of ethanol dehydration, i.e. acetaldehyde, was not observed; however, no control was performed on pure acetaldehyde to make sure it was able to be resolved from the ethanol peak.

To attempt to answer the question of whether the hydrogen atoms in the produced H_2 gas come from ethanol or water, a series of experiments using deuterated solvents were conducted. After photolysis, the entire reactor headspace was recirculated through a mass spectrometer. The initial appearance of As this was not a high-resolution isotope mass spectrometer, since both D^+ and H_2^+ ions are mass 2, only HD and D_2 could be compared. In the first experiment, 25 mL of D_2O (99.9%, Cambridge Isotopes) and 25

mL of ethanol were used as the reaction solution. The observed ratio of HD to D₂ was found to be 1.8 to 1. As it is possible for proton exchange to occur between water and the ethanol –OH proton (which is known to be acid or base catalyzed), the isotopic composition of water needed to be varied in order to see the contribution of proton exchange in the observed isotopic product ratios. In the second experiment, 12.5 mL of H₂O and 12.5 mL of D₂O were used, along with 25 mL of ethanol. The observed ratio of HD to D₂ was found to be 9.5 to 1. As expected, proton exchange between water and ethanol was observed, as signals were seen for gas-phase H₂O, HDO, D₂O, C₂H₅OH and C₂H₅OD for all experiments. Assuming all protons for hydrogen production come from either water or the ethanol –OH proton, and assuming complete proton exchange between water and ethanol, and ignoring for the moment any kinetic isotope effect, the ratio of HD to D₂ can be calculated from the probability of whether a random available proton is H or D. For the first experiment, the actual molar concentration of each solvent was approximately 27.5 mol/L water and 8.6 mol/L ethanol. Thus, roughly 7/8 of all available protons would be D, and the remaining 1/8 would be H. Since either HD or DH can be made, the probability of a species with one H atom and one D atom is $1/8 * 7/8 + 7/8 * 1/8$ which is about 1/4. Similarly, the probability of making D₂ would be $7/8 * 7/8$ which is about 3/4. Thus, the expected product ratio of HD to D₂ would be about 1 to 3, or .3. However, the observed ratio was 1.8 to 1, indicating that at least one of the assumptions is faulty. Similarly, the expected ratio for the second experiment also differs greatly from the experimentally observed ratio.

Some possible explanations are as follows. It is very likely the alpha hydrogens from carbon-hydrogen bonds in ethanol could be abstracted to form H₂. Thus, a

worthwhile future experiment would be to use a deuterated ethanol with isotopically labeled alpha protons (such as $\text{CH}_3\text{CD}_2\text{OH}$) in conjunction with H_2O , and to check for HD and D_2 . The rate-limiting step for hydrogen production, which is most likely proton abstraction from either water or ethanol, will also exhibit a kinetic isotope effect (KIE) whose magnitude will depend on the position of the proton in the transition state. For hydroxyl radical abstraction of ethanol alpha hydrogens, this value is known to be approximately 2.²⁵ However, this value can certainly be much higher depending on the nature of the hydrogen abstraction reaction in our system. To properly isolate the contribution of the KIE, a control experiment using non-deuterated solvents needs to be run in conjunction with an experiment using completely $-\text{OD}$ deuterated solvents, as well as another experiment using fully deuterated ethanol ($\text{C}_2\text{D}_5\text{OD}$). The overall hydrogen production would be quantified by the usual GC-TCD method, and the KIE can then be calculated for both the $-\text{OH}$ abstraction pathway as well as the $-\text{CH}$ abstraction pathway.

Another possible explanation is that proton exchange in solution between ethanol and water should be rapid, but at the catalyst surface, it is possible that exchange is slowed down or even completely stopped. And yet another possibility is that protons from the catalyst itself are reduced to H_2 . We have seen evidence for a Ni-H species from NMR data, and since we believe Ni plays an important role as an electron sink, hydrogen production likely occurs near Ni atoms, and thus near a source of H atoms.

Figure 5.5 shows the XPS data for the Cd $3d^{5/2}$ and $3d^{3/2}$ states in CdS/Ni/ KNbO_3 before and after photolysis. Two distinct forms of Cd are observed, and the ratio of the two changes after the photoreaction. Note that no change in Nb peak shape was seen. The higher-energy peaks in each pairing (413.6 and 406.9 eV) are assigned to CdS, and

the lower-energy peaks (412.8 and 406.0 eV) are assigned to Cd-substituted niobate sites, which would have CdO character. Reference data indicates CdS to have a binding energy between 0.7 to 1.1 eV higher than CdO,²⁶ which is consistent with the 0.8 to 0.9 eV difference in peak positions. Using the Nb peak to normalize the relative peak areas between the two samples (the overall Nb content should not change), it was found that there was a 25% loss of Cd that occurred during photolysis, but no net loss of sulfur (the XPS sulfur signal was too weak to perform individual peak assignment, only total area could be measured). The loss in intensity is seen as a reduction in the CdO peak, which can be explained as follows. It is likely that not all Cd substitution sites were accessible for formation of CdS, and thus remained in the niobate matrix as Cd counterions. The Cd at these substitution sites could then leech out of the catalyst during the 24-hour reaction period. Another possibility is that the Cd loss was actually from CdS particles that had been photocorroded, but that the sulfur atoms stayed behind.

K₄Nb₆O₁₇

Figure 5.6 shows the SEM images of the composite CdS/Ni/K₄Nb₆O₁₇ catalyst. The particle size is large, on the order of a few microns, and individual layers of submicron thickness can be clearly seen. The BET surface area was measured at 1.0 m²/g, consistent with the large particle size. The SEM images also show the presence of large aggregates on the surface of the particles, which may be absorbed CdS particles. The images also contain smaller dotlike structures on the surface, which are likely Ni/NiO islands.

Figure 5.7 shows the UV/vis diffuse reflectance spectra of both the starting K₄Nb₆O₁₇ material and the CdS/Ni/K₄Nb₆O₁₇ catalyst. The absorption edge is seen to

stretch into the visible region, between 400 and 500 nm, as expected for a visible light catalyst. Figure 5.8 shows the results of the hydrogen evolution experiments. The order of catalytic activity was CdS/Ni/KNbO_3 ($k = 23.5 \mu\text{mol H}_2 \text{ hr}^{-1}$) > $\text{CdS/Ni/K}_4\text{Nb}_6\text{O}_{17}$ ($k = 7.3 \mu\text{mol H}_2 \text{ hr}^{-1}$) > $\text{CdS/K}_4\text{Nb}_6\text{O}_{17}$ ($k = 2.8 \mu\text{mol H}_2 \text{ hr}^{-1}$) > $\text{CdS/Ni/H}^+/\text{K}_4\text{Nb}_6\text{O}_{17}$ ($k = .3 \mu\text{mol H}_2 \text{ hr}^{-1}$). Given the problems observed during the synthesis of the proton exchanged catalyst, the low amount of hydrogen production from this material was not surprising. The increased activity with Ni doping is consistent with our earlier work on KNbO_3 .⁹

Figure 5.9 shows the DRIFT spectra of the starting $\text{K}_4\text{Nb}_6\text{O}_{17}$ material, the two best-performing modified $\text{K}_4\text{Nb}_6\text{O}_{17}$ catalysts, as well as a post-reaction catalyst that was recovered after a 24-hour photolysis experiment. The appearance of a sharp peak in the two pre-photoreaction catalysts at 1110 cm^{-1} is assigned to CdS. Post-photoreaction, this peak is seen to disappear, indicating the loss of all IR-active CdS.

Figure 5.10 shows XPS data for the Cd $3d^{5/2}$ and $3d^{3/2}$ states in $\text{CdS/Ni/K}_4\text{Nb}_6\text{O}_{17}$ before and after photolysis. As in the case of CdS/Ni/KNbO_3 , two distinct forms of Cd are observed, and the ratio of the two changes after the photoreaction. Unlike the KNbO_3 catalysts, however, there is a large loss of both Cd (70%) and S (45%) during the course of the photoreaction. Given the disappearance of the CdS signal from the FTIR, the loss of much of the CdS is not surprising. However, it appears that some CdS still remains behind, as indicated by the presence of the higher-energy Cd peak that is present in both the pre- and post-reaction catalyst. It may be that this remaining CdS is in an IR inactive state or in too little amount to be detected; or, it is possible that indeed no CdS is left, and

that the remaining sulfur is in the form of elemental sulfur. Unfortunately, the sulfur XPS signal was too weak to perform analysis of sulfur oxidation states.

Another series of XPS experiments was performed to examine the effect of Ni doping on the subsequent CdS doping to the $K_4Nb_6O_{17}$ catalyst. Comparatively, 30% less CdS was seen on the CdS/Ni/ $K_4Nb_6O_{17}$ catalyst compared to the CdS/ $K_4Nb_6O_{17}$ catalyst. Given that Ni likely competes with Cd for ion exchange sites, this result is not surprising, as many of the potential sites for Cd ion exchange were likely blocked by the prior Ni ion exchange.

Conclusions

The niobium oxides KNbO_3 and $\text{K}_4\text{Nb}_6\text{O}_{17}$ can both be combined with nanoparticulate CdS particles and Ni to produce H_2 gas from water/ethanol solutions using visible light. The chemical environment of Ni, whether surface-bound or incorporated into the catalyst structure, has an affect on Nb–O bonds. Ni doping increases the catalytic efficiency even though there is less overall CdS in the catalyst as compared to a non-Ni doped catalyst. During the course of the photoreaction, KNbO_3 catalysts were seen to lose Cd ions, likely leached from counterion sites in the niobate matrix. On the other hand, $\text{K}_4\text{Nb}_6\text{O}_{17}$ catalysts were seen to lose a significant amount of CdS from photolysis. Loss of CdS is a significant problem, and any future efforts must use novel methods for CdS implantation into the catalyst to prevent loss of photocatalytic activity.

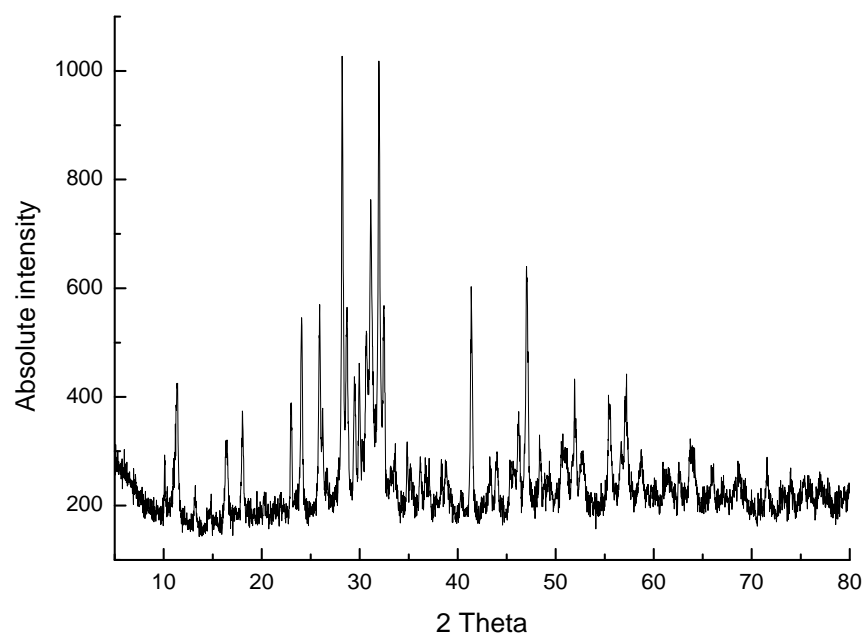


Figure 5.1. XRD spectrum of $K_4Nb_6O_{17}$.

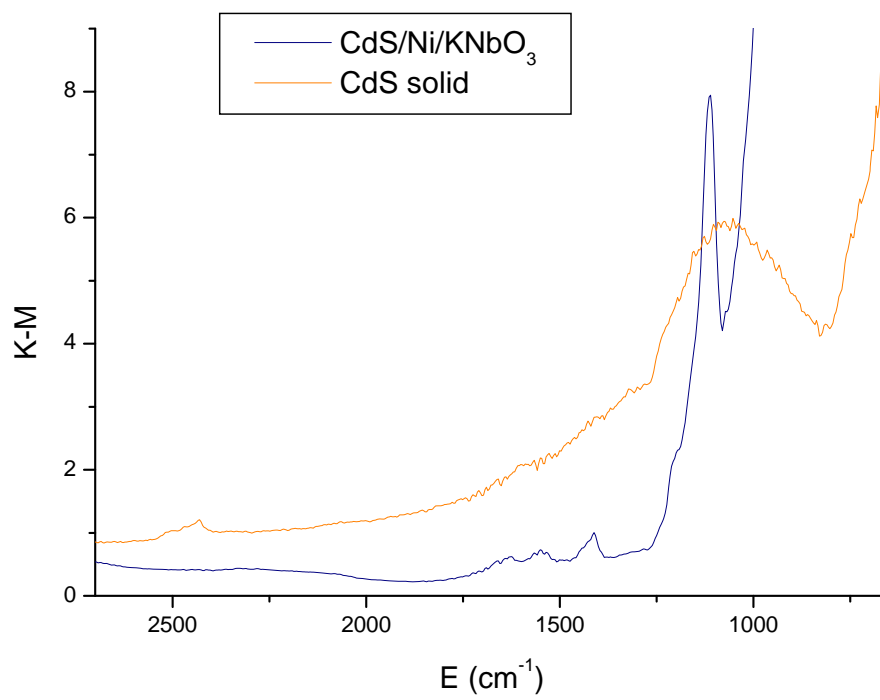


Figure 5.2. DRIFT spectra for CdS/Ni/KNbO_3 and solid CdS .

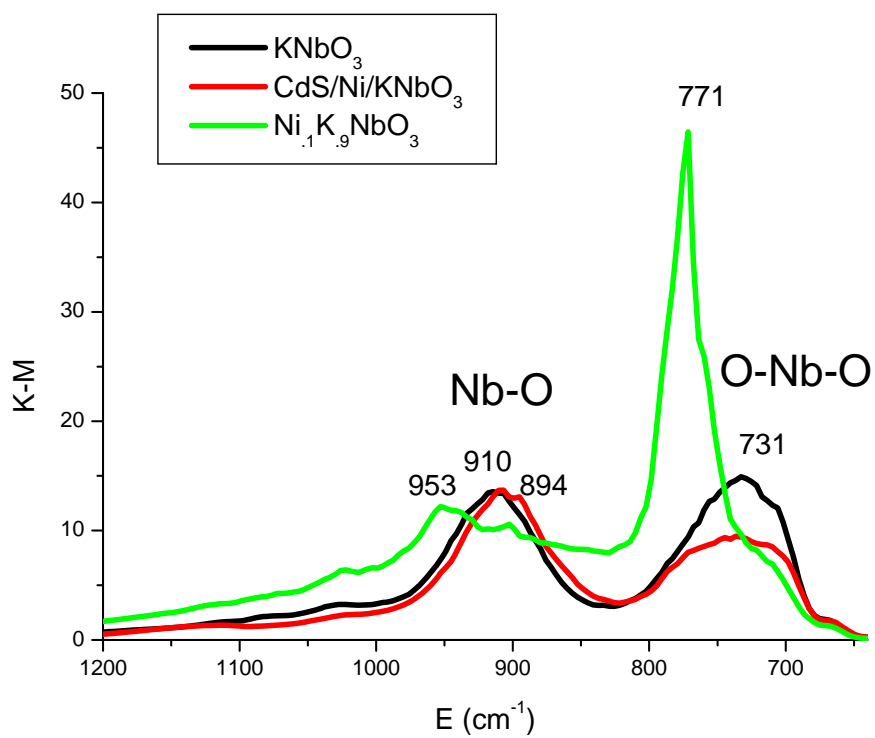


Figure 5.3. DRIFT spectra for KNbO_3 , CdS/Ni/KNbO_3 , and $\text{Ni}_{1.1}\text{K}_{0.9}\text{NbO}_3$.

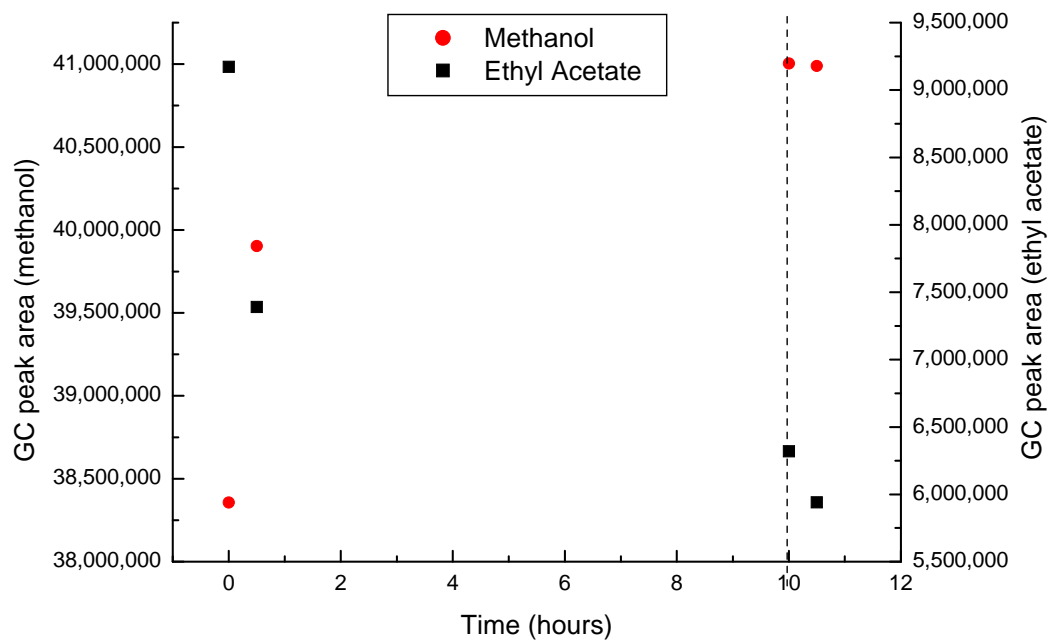


Figure 5.4. GC/MS data for species in solution during course of the reaction. Dashed vertical line indicates when the lamp was turned off and the reaction mixture exposed to air.

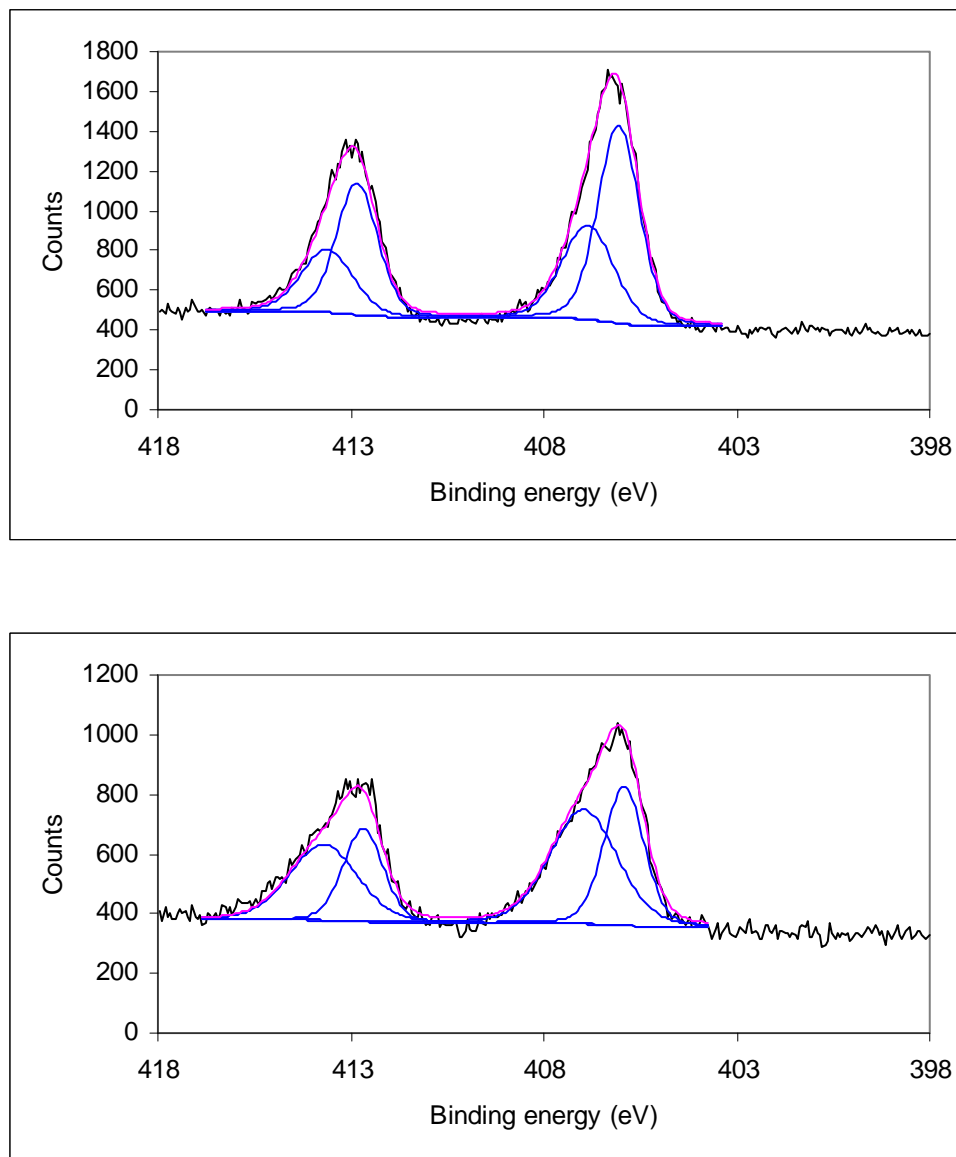


Figure 5.5. XPS of Cd peaks from CdS/Ni/KNbO₃ before (top) and after (bottom) photoreaction.

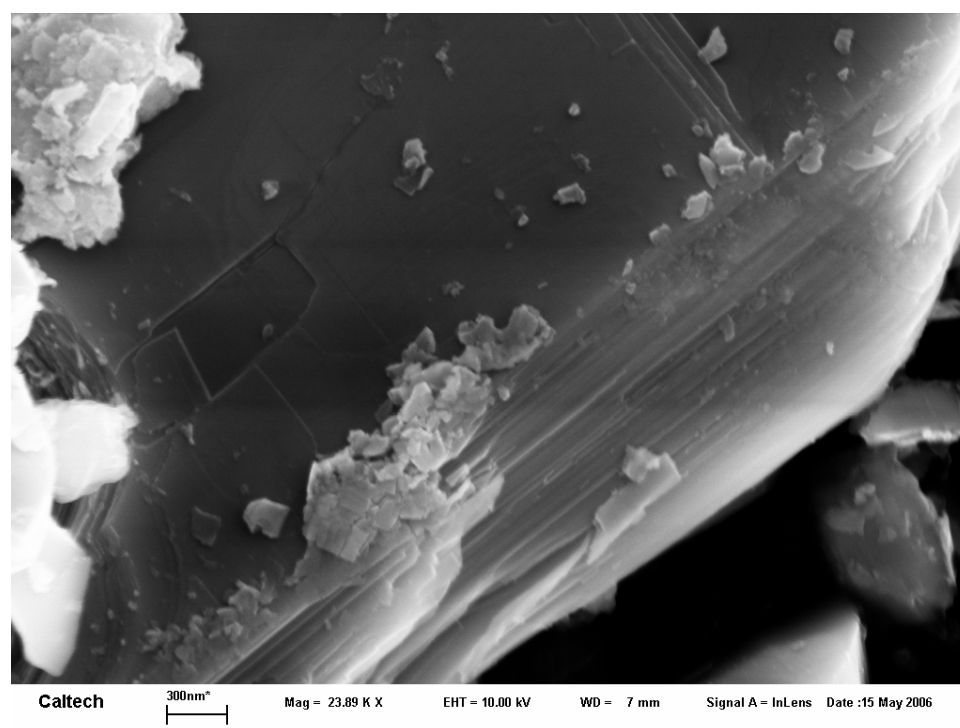
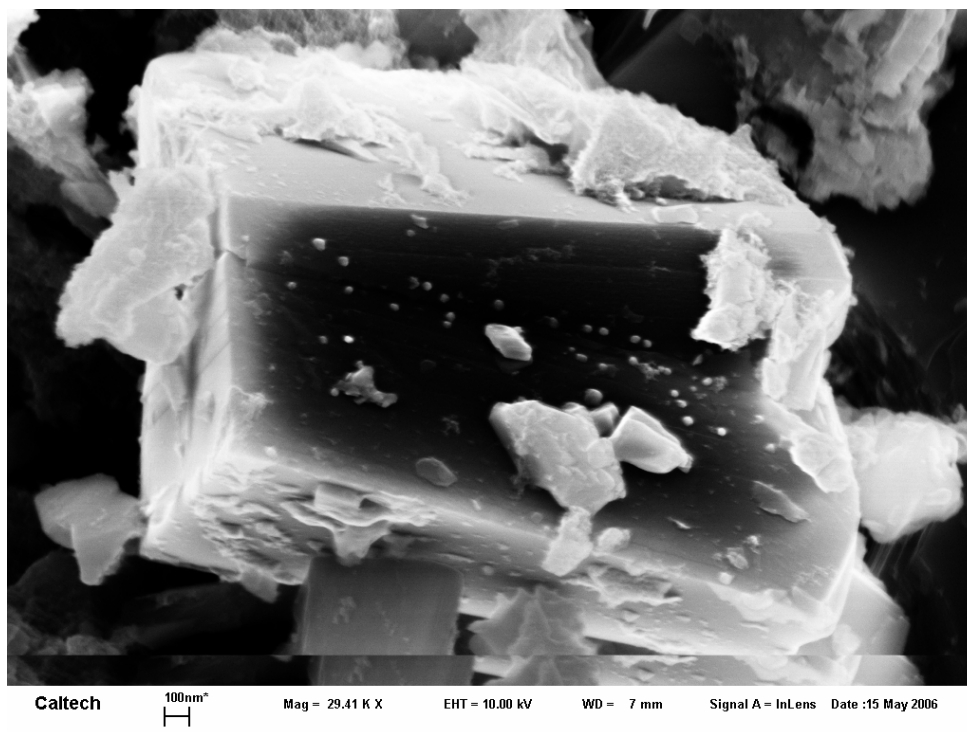


Figure 5.6. SEM images of CdS/Ni/K₄Nb₆O₁₇.

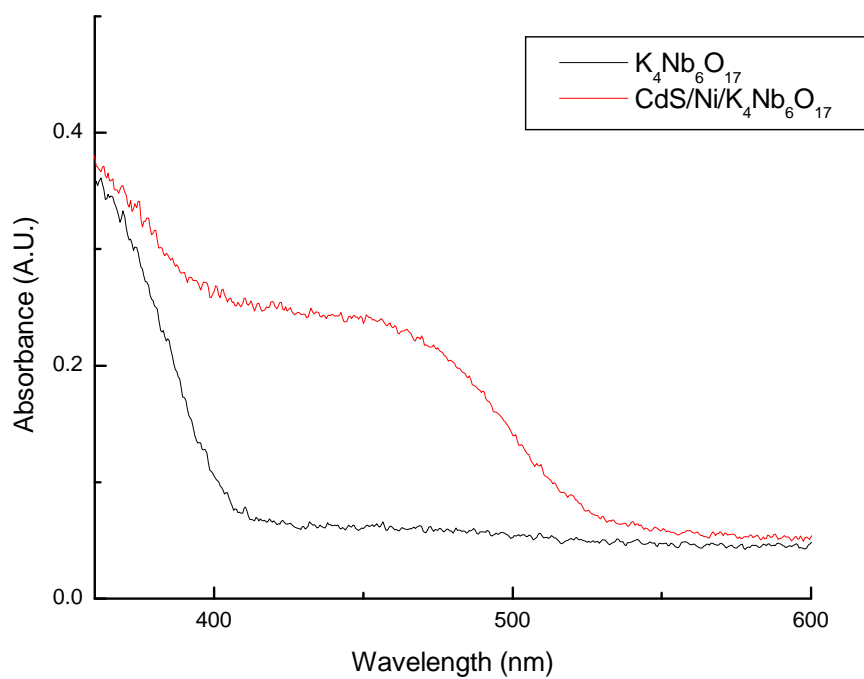


Figure 5.7. UV-vis diffuse reflectance spectra of $K_4Nb_6O_{17}$ and $CdS/Ni/K_4Nb_6O_{17}$.

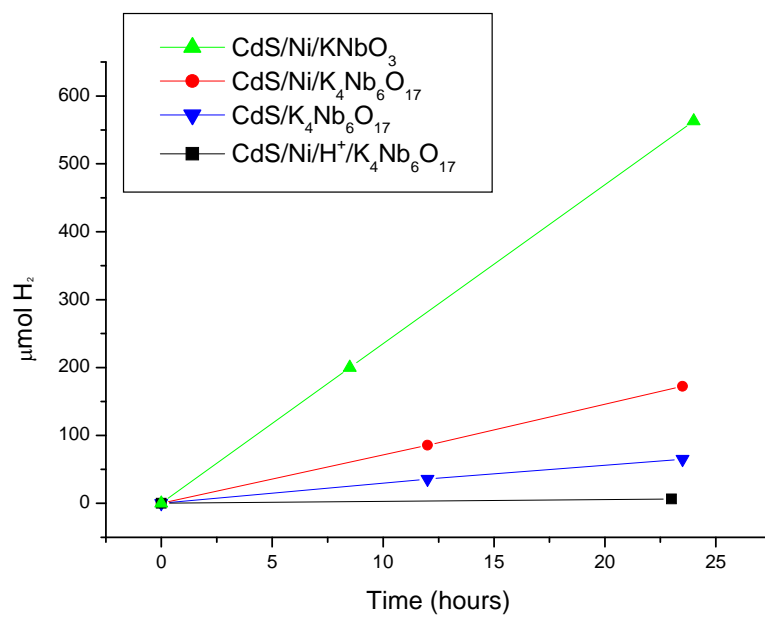


Figure 5.8. Hydrogen production rates for CdS/Ni/KNbO₃, CdS/Ni/K₄Nb₆O₁₇, CdS/K₄Nb₆O₁₇ and CdS/Ni/H⁺/K₄Nb₆O₁₇.

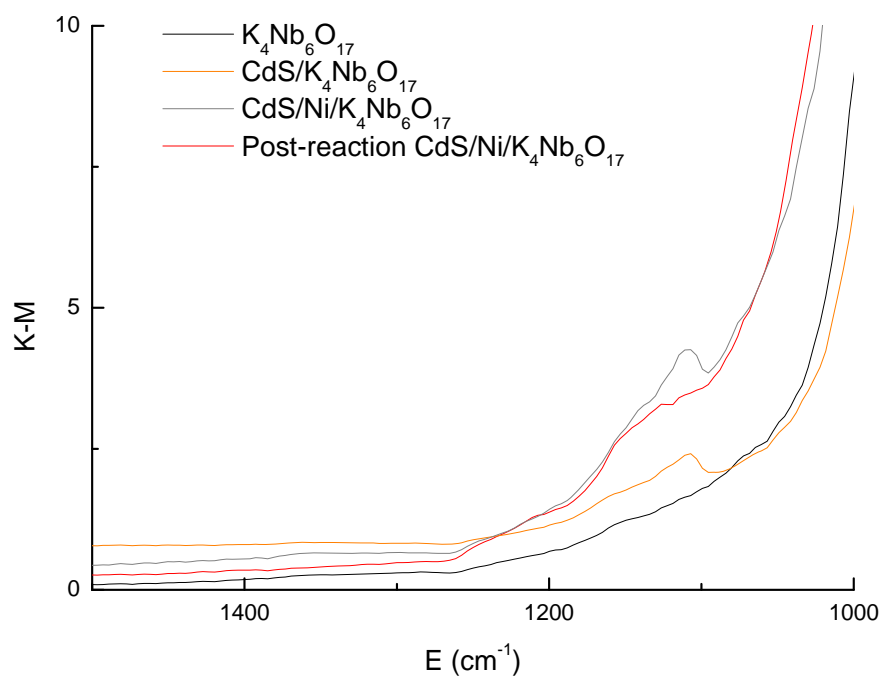


Figure 5.9. DRIFT spectra for $K_4Nb_6O_{17}$, $CdS/K_4Nb_6O_{17}$, $CdS/Ni/K_4Nb_6O_{17}$ and post-reaction $CdS/Ni/K_4Nb_6O_{17}$.

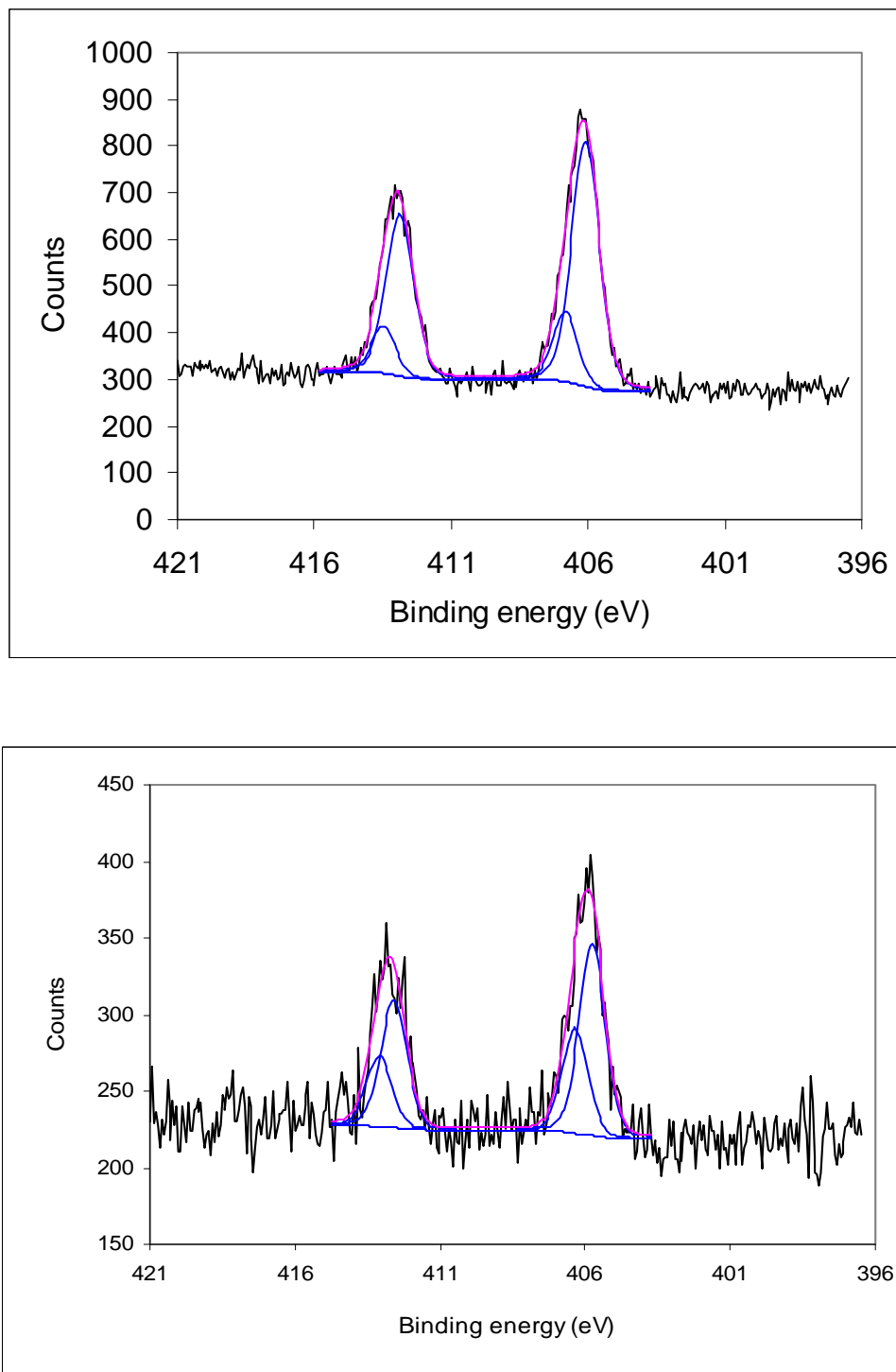


Figure 5.10. XPS of Cd peaks from CdS/Ni/K₄Nb₆O₁₇ before (top) and after (bottom) photoreaction.

References

- (1) Zhang, G.; Ouyang, S.; Liu, H. Preparation method for photocatalyst of niobium potassium oxide; (Wuhan University of Technology, Peop. Rep. China). China, 2005; pp 6.
- (2) Hayashi, H.; Hakuta, Y.; Kurata, Y. *J. Mater. Chem.* **2004**, *14*, 2046.
- (3) Gasperin, M.; Lebihan, M. T. *J. Solid State Chem.* **1980**, *33*, 83.
- (4) Kudo, A.; Sakata, T. *J. Phys. Chem.* **1996**, *100*, 17323.
- (5) Domen, K.; Kudo, A.; Shibata, M.; Tanaka, A.; Maruya, K.; Onishi, T. *J. Chem. Soc., Chem. Commun.* **1986**, 1706.
- (6) Kudo, A.; Tanaka, A.; Domen, K.; Maruya, K.; Aika, K.; Onishi, T. *J. Catal.* **1988**, *111*, 67.
- (7) Yuan, J.; Chen, K.; Chen, M.; Shang, G. *Taiyangneng Xuebao* **2005**, *26*, 811.
- (8) Yoshimura, J.; Tanaka, A.; Kondo, J. N.; Domen, K. *Bull. Chem. Soc. Jpn.* **1995**, *68*, 2439.
- (9) Choi, J.; Ryu, S. Y.; Balcerski, W.; Hoffmann, M. R. **2006**, COLL.
- (10) Davis, A. P.; Huang, C. P. *Water Res.* **1991**, *25*, 1273.
- (11) Korgel, B. A.; Monbouquette, H. G. *J. Phys. Chem. B* **1997**, *101*, 5010.
- (12) Vucemilovic, M. I.; Vukelic, N.; Rajh, T. *Photochem. Photobiol., A* **1988**, *42*, 157.
- (13) Tang, W. Z.; Huang, C. P. *Water Res.* **1995**, *29*, 745.
- (14) Davis, A. P.; Hsieh, Y. H.; Huang, C. P. *Chemosphere* **1994**, *28*, 663.
- (15) Hsieh, Y. H.; Huang, C. P.; Davis, A. P. *Chemosphere* **1993**, *27*, 721.

- (16) Hsieh, Y. H.; Huang, C. P.; Davis, A. P. *Chemosphere* **1992**, *24*, 281.
- (17) Hsieh, Y. H.; Huang, C. P. *Colloids Surf.* **1991**, *53*, 275.
- (18) Liu, J.-F.; Li, X.-L.; Li, Y.-D. *J. Cryst. Growth* **2003**, *247*, 419.
- (19) Uchida, S.; Inoue, Y.; Fujishiro, Y.; Sato, T. *J. Mater. Sci.* **1998**, *33*, 5125.
- (20) Kudo, A.; Sayama, K.; Tanaka, A.; Asakura, K.; Domen, K.; Maruya, K.; Onishi, T. *J. Catal.* **1989**, *120*, 337.
- (21) Abe, R.; Shinohara, K.; Tanaka, A.; Hara, M.; Kondo, J. N.; Domen, K. *J. Mater. Res.* **1998**, *13*, 861.
- (22) Yao, K.; Nishimura, S.; Imai, Y.; Wang, H.; Ma, T.; Abe, E.; Tateyama, H.; Yamagishi, A. *Langmuir* **2003**, *19*, 321.
- (23) Kaito, R.; Kuroda, K.; Ogawa, M. *J. Phys. Chem. B* **2003**, *107*, 4043.
- (24) Abe, R.; Shinohara, K.; Tanaka, A.; Hara, M.; Kondo, J. N.; Domen, K. *Chem. Mater.* **1997**, *9*, 2179.
- (25) Bonifacic, M.; Armstrong, D. A.; Stefanic, I.; Asmus, K. D. *J. Phys. Chem. B* **2003**, *107*, 7268.
- (26) Wagner, C. D.; Naumkin, A. V.; Kraut-Vass, A.; Allison, J. W.; Powell, C. J.; Rumble Jr., J. R. NIST X-ray Photoelectron Spectroscopy Database; Measurement Services Division of the National Institute of Standards and Technology, 2006.